
14 Apr 2023

Effects of Autoionizing Resonances on Wave-Packet Dynamics Studied by Time-Resolved Photoelectron Spectroscopy

Pengju Zhang

Van Hung Hoang

Chuncheng Wang

Tran Trung Luu

et. al. For a complete list of authors, see https://scholarsmine.mst.edu/phys_facwork/2306

Follow this and additional works at: https://scholarsmine.mst.edu/phys_facwork

 Part of the [Physics Commons](#)

Recommended Citation

P. Zhang et al., "Effects of Autoionizing Resonances on Wave-Packet Dynamics Studied by Time-Resolved Photoelectron Spectroscopy," *Physical Review Letters*, vol. 130, no. 15, article no. 153201, American Physical Society, Apr 2023.

The definitive version is available at <https://doi.org/10.1103/PhysRevLett.130.153201>

This Article - Journal is brought to you for free and open access by Scholars' Mine. It has been accepted for inclusion in Physics Faculty Research & Creative Works by an authorized administrator of Scholars' Mine. This work is protected by U. S. Copyright Law. Unauthorized use including reproduction for redistribution requires the permission of the copyright holder. For more information, please contact scholarsmine@mst.edu.

Effects of Autoionizing Resonances on Wave-Packet Dynamics Studied by Time-Resolved Photoelectron Spectroscopy

Pengju Zhang,^{1,*†} Van-Hung Hoang^{2,3,*} Chuncheng Wang,^{1,‡} Tran Trung Luu,^{1,4} Vít Svoboda,^{1,§}
Anh-Thu Le,^{2,5,||} and Hans Jakob Wörner¹

¹Laboratory for Physical Chemistry, ETH Zürich, Vladimir-Prelog-Weg 2, 8093 Zürich, Switzerland

²Department of Physics, Missouri University of Science and Technology, Rolla, Missouri 65409, USA

³Department of Physics, Kansas State University, Manhattan, Kansas 66506, USA

⁴Department of Physics, The University of Hong Kong, Pokfulam Road, SAR Hong Kong, People's Republic of China

⁵Department of Physics, University of Connecticut, 196A Auditorium Road, Unit 3046, Storrs, Connecticut 06269, USA



(Received 10 June 2022; accepted 23 February 2023; published 12 April 2023)

We report a combined experimental and theoretical study on the effect of autoionizing resonances in time-resolved photoelectron spectroscopy. The coherent excitation of N₂ by ~14.15 eV extreme-ultraviolet photons prepares a superposition of three dominant adjacent vibrational levels ($v' = 14-16$) in the valence $b' \ ^1\Sigma_u^+$ state, which are probed by the absorption of two or three near-infrared photons (800 nm). The superposition manifests itself as coherent oscillations in the measured photoelectron spectra. A quantum-mechanical simulation confirms that two autoionizing Rydberg states converging to the excited $A \ ^2\Pi_u$ and $B \ ^2\Sigma_u^+ N_2^+$ cores are accessed by the resonant absorption of near-infrared photons. We show that these resonances apply different filters to the observation of the vibrational wave packet, which results in different phases and amplitudes of the oscillating photoelectron signal depending on the nature of the autoionizing resonance. This work clarifies the importance of resonances in time-resolved photoelectron spectroscopy and particularly reveals the phase of vibrational quantum beats as a powerful observable for characterizing the properties of such resonances.

DOI: [10.1103/PhysRevLett.130.153201](https://doi.org/10.1103/PhysRevLett.130.153201)

Photoinduced wave-packet dynamics is one of the central topics in femtochemistry [1] and attosecond physics [2]. A wave packet is formed whenever a coherent superposition of several eigenstates is prepared [3–10]. The corresponding wave-packet dynamics can be effectively studied using time-resolved pump-probe spectroscopy. A particularly powerful method to probe such dynamics is time-resolved photoelectron spectroscopy (TRPES), owing to its sensitivity to both electronic and structural dynamics [11–15].

An important open question in TRPES is the role of resonances in the probe step on the observed dynamics. Such resonances are the rule rather than the exception when ionization is performed with long-wavelength, in particular visible or ultraviolet, light sources. Resonances can occur as an intermediate step in multiphoton absorption or at the final step in both single- and multiphoton absorption. Previous evidence suggests that intermediate resonances can lead to significant differences in the time-dependent signals. For example, a recent study of perylene has shown evidence of a subpicosecond relaxation dynamics when probed through resonance-enhanced multiphoton ionization, whereas no such relaxation was visible when single-photon probing was used [16]. Similarly, a recent study of the excited-state dynamics in SO₂ using three-photon ionization at 400 nm found pronounced vibronic wave-packet dynamics [17], whereas a single-photon TRPES

study did not observe such dynamics [18]. In both perylene and SO₂, it is likely that the presence of intermediate resonances is responsible for the different time-dependent signals obtained from probing the same wave-packet dynamics via different ionization pathways.

In comparison to the case of intermediate resonances, the case of final, autoionizing resonances is even less understood. These autoionizing resonances are likely to contribute to most TRPES studies in which ionization is performed within a few electron volts of the threshold because of the presence of dense series of Rydberg states converging to the electronically excited states of the molecular cation. To fully characterize and understand the effect of such resonances, it is desirable to select a system with a well-known electronic structure, such that all states can be assigned and which is simple enough that the effect of different resonances can be fully resolved. Moreover, the system should support clear and long-lived wave-packet dynamics that can then be probed through different resonances, highlighting their specific roles in the TRPES probe step. Adding the knowledge gained from recent time-resolved studies of N₂ [19–25], we identified this system as a promising candidate for the present study.

In this Letter, we report a combined experimental and theoretical study of time-dependent wave-packet dynamics in N₂ prepared by broadband extreme ultraviolet (XUV)

(14.15 ± 0.07 eV) excitation and probed by two or three near-infrared (NIR) photons, accessing several autoionizing resonances. The broadband XUV excitation, the short cross-correlation time, and the vibrationally resolved TRPES allow us to observe (i) quantum beats between three dominant high-lying vibrational levels within the same electronic state and (ii) the dependence of the phase and amplitude of these quantum beats on the autoionizing Rydberg states above the first ionization threshold populated by the probe laser.

The experimental setup was previously described in Ref. [26]. A fundamental NIR pulse (800 nm, 30 fs, 5 kHz) was divided by a beam splitter (70:30). The major portion (~0.5 mJ) was used for high-harmonic generation, providing the XUV-pump (H9) pulse. The minor portion, serving as the probe pulse, was independently focused on the gas jet in the second arm of the interferometer. The time delay between the XUV-pump and NIR-probe pulses was scanned between -130 and +2150 fs in steps of 10 fs. The XUV NIR cross correlation of ~50 fs was determined through by the laser-assisted photoelectric effect [27] of carbon dioxide ionized by a (1 + 1') scheme. The NIR probe intensity of 2×10^{12} W/cm² was estimated based on the Stark shift of the photoelectron bands. The advantage of the selected pump-probe scheme is that no single-photon (XUV or NIR) ionization event is observed, thus providing a background-free scheme with only pump-probe pathways contributing to the signal.

The experimental results were simulated using the coupled-channel time-dependent Schrödinger equation for N₂ interacting with pump and probe laser pulses. Our theoretical method was reported earlier [28]. For the treatment of photoelectrons, we follow the method proposed in Refs. [29–31]. We included the N₂ ground electronic state ($X^1\Sigma_g^+$), as well as several excited electronic states based on their symmetries and energies. Specifically, we included the diabatic states b' , c' , and e' of $1^1\Sigma_u^+$ symmetry, around 14 eV above the ground state in the Franck-Condon (FC) region [32–34], which couple strongly with the ground state by the pump pulse. Diabatic states b , c , and o of $1^1\Pi_u$ symmetry, which also have energies near 14 eV were not taken into account since they play a less important role as confirmed by the experiment. Moreover, two Rydberg states, $4p\pi_u(1^1\Sigma_g^+)$ converging to $A^2\Pi_u$ and $4s\sigma_g(1^1\Sigma_g^+)$ [35] converging to $X^2\Sigma_g^+$, were included because they are accessed by the probe pulse. In addition, the autoionizing Rydberg states $3d\sigma_g(1^1\Sigma_u^+)$ converging to $B^2\Sigma_u^+$, and $11d\sigma_g$ [36,37] converging to $A^2\Pi_u$, were included as well since they couple to the intermediate b' state by a two-photon transition and are enhanced by a resonance at 17.15 eV ($v = 0$) and at 17.25 eV ($v = 3$), respectively. These autoionizing states decay to the ground electronic state of N₂⁺ ($X^2\Sigma_g^+$), which is also included in the calculation.

The diagonal matrix elements of the Hamiltonian are $H_{ii} = T_R + V_{ii}$, where $T_R = -(\partial^2/2\mu\partial R^2)$ is the nuclear

kinetic energy operator and $V_{ii}(R)$ is the potential energy of channel i . The dynamic ponderomotive energy $U_p(t)$ is added to the energies of the highest three channels, and the electron kinetic energy $E = k^2/2$ is added to the ionic state energy. The off-diagonal matrix elements are $H_{ij} = \vec{E}(t) \cdot \vec{d}_{ij}(R) + V_{ij}(R)$, where $\vec{d}_{ij}(R)$ is the dipole coupling between channels i and j and V_{ij} is the electronic coupling of different diabatic states. The potential energy curves (PECs) illustrated in Fig. 3 and transition dipoles are taken from Refs. [33,38] and Refs. [33,39], respectively. The XUV (NIR) pulse is modeled with a Gaussian envelope with the duration of 25 fs (40 fs) and photon energy of 14.15 eV (1.55 eV). The pump-probe photoelectron spectrum is calculated as

$$S(E) = \sum_i \int |\chi_i(R, E)|^2 dR, \quad (1)$$

where $\chi_i(R, E)$ is a nuclear wave function, and the sum is taken over the ionic state channels.

Figure 1(b) shows the experimental two-dimensional (2D) TRPES, and the corresponding one-dimensional (1D) photoelectron spectrum integrated over all the time delays is shown in Fig. 1(a). The spectrum is truncated around 0.3 eV due to the maximum acquisition time window of the time-of-flight device. In Fig. 1(b), no photoelectron signals are observed prior to time zero, and two distinct groups of photoelectron signals showing up during the cross-correlation. Peaks below 1.66 eV are assigned to the transition of one XUV plus two NIR photons, whereas peaks above 1.66 eV correspond to one XUV plus three NIR photons. An intuitive mechanism behind the observation is depicted in Fig. 3. From here on, we mainly focus on the discussion of the spectra induced by the absorption of two NIR photons.

The two-NIR-photon region is dominated by a peak around 1.55 eV assigned to a transition from the neutral ground state to the $b' 1^1\Sigma_u^+$ valence state (XUV pump), which is subsequently excited to the Rydberg state $3d\sigma_g$ ($v' = 0$) [36,37,40] (NIR probe). This state autoionizes to the ionic ground state $X^2\Sigma_g^+$ ($v'' = 0$). Similarly, the second-strongest peak around 1.66 eV is assigned to the autoionization of the Rydberg state $11d\sigma_g$ ($v' = 3$) [36] to $X^2\Sigma_g^+$ ($v'' = 0$). The measured energy difference of 0.11 eV between these two peaks verifies the corresponding energy gap between the respective Rydberg states. In the same way, three pairs of peaks below 1.55 eV are assigned as transitions to $X^2\Sigma_g^+$ ($v'' = 1, 2, 3$). Two extra peaks assigned as transitions from autoionization of the Rydberg state $8d\pi_g$ ($v' = 3$) [36,37,41,42] to $X^2\Sigma_g^+$ ($v'' = 2, 3$) also appear in this region.

The previously discussed peaks have also different time evolutions. Around time zero, all signals from different Rydberg states appear at the same time. After the cross-correlation time, the signal from the $11d\sigma_g$ ($v' = 3$) state

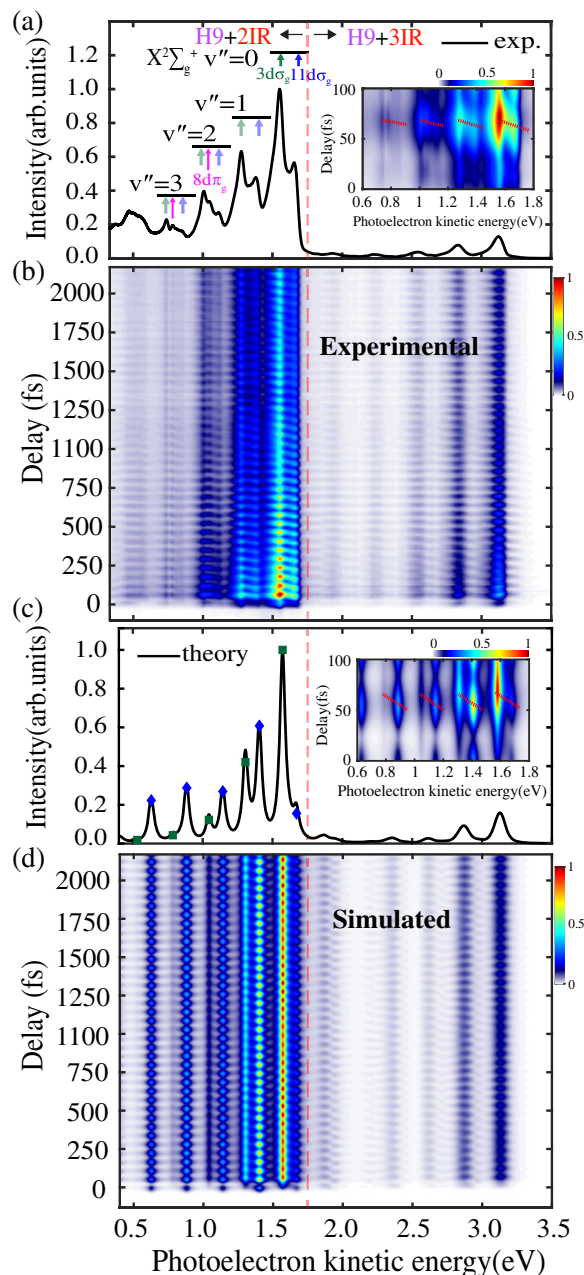


FIG. 1. (a) Delay-Integrated measured and (c) simulated photoelectron spectrum of N_2 following XUV (H9) pump excitation and NIR (800 nm) multiphoton absorption, the peak assignments for two-NIR-photon absorption are shown on the top. (b) Experimental and (d) simulated 2D TRPES. The region from 0 to 100 fs is enlarged in the insets of (a) and (c), respectively. Positive delay signifies that the NIR probe pulse follows the XUV pump pulse. The simulated photoelectron spectra are convoluted with a 40-meV Lorentzian line shape. The FC factors for subpeaks (blue diamonds) and main peaks (green squares) are shown in (c), respectively.

shows up before the one from the $3d\sigma_g$ ($v' = 0$) state [see the inset in Fig. 1(a)], and the spectrum exhibits clear beating with a period of about 50 fs. Moreover, the relative time difference between $11d\sigma_g$ ($v' = 3$) and $3d\sigma_g$ ($v' = 0$)

to $X^2\Sigma_g^+$ ($v'' = 0, 1, 2, 3$) amount to 12.0 ± 1.2 fs, 9.7 ± 0.8 fs, 7.7 ± 1.0 fs, and 2.7 ± 0.8 fs, respectively (see the red dashed lines in the inset of Fig. 1(a) and the Fig. S1 in Supplemental Material [43]). In the following, the signal originating from $3d\sigma_g$ ($v' = 0$) and $11d\sigma_g$ ($v' = 3$) is referred to as “main peaks” and “subpeaks,” respectively.

Figure 1(c) shows the calculated photoelectron spectrum. The calculation reproduces all main features from the measured spectrum well in both the two-NIR-photons and three-NIR-photons regions. The main and subpeaks are clearly visible in the calculation and their positions correspond to the measured peaks within 0.02 eV. However, the intensity ratio between the main and subpeaks differs between the calculation and the experiment. This is mainly due to an incomplete evaluation of the FC factors in the theory, shown as blue diamonds (subpeaks) and green squares (main peaks), respectively. The calculations also underestimate the photoelectron background in the region of 0.3–1.5 eV, which we attribute to the fact that the direct-ionization (as opposed to the autoionization) channels are not included. Figure 1(d) shows the calculated 2D spectrum which can be directly compared with Fig. 1(b). The calculations predict clear beating signals for all main and subpeaks in the two-NIR-photons region in excellent agreement with the experiment. We note that the amplitude of the calculated beating signal is constant, whereas it decays in the experiment as a consequence of rotational dynamics that are not included in the calculations.

Time-dependent profiles for main and subpeaks are shown in Figs. 2(a) and 2(b), respectively. All traces have similar time profiles with a well-resolved beating pattern and an exponential intensity decay. The beating pattern is encoded into amplitude revivals which depend on time delay. This is due to the anharmonicity of the $b' \ ^1\Sigma_u^+$ PEC [44,45] causing nonequidistant vibrational level spacings. Therefore, the initially well-localized wave packet dephases and partially rephases over time. The exponential intensity decay is characterized with a single time constant of ~ 8 ps, which is in good agreement with an expected value derived from the known rotational constant of the $b' \ ^1\Sigma_u^+$ state [42,46], and the assumption that the XUV excitation prepares a certain degree of rotational coherence, which later undergoes dephasing and overall decrease of the measured beating signal.

Figures 2(c) and 3(d) show Fourier analysis of both experimental and theoretical 2D spectra, respectively, providing further insights into the nuclear dynamics. The main peaks have two dominant frequencies: one around 17.5 THz corresponding to beating between b' ($v' = 15$) and ($v' = 16$) states and the other around 18.8 THz corresponding to beating between b' ($v' = 14$) and ($v' = 15$) states, shown as an inset in Fig. 2(a). Identification of these two beating frequencies confirms our assignment that three adjacent vibronic levels are

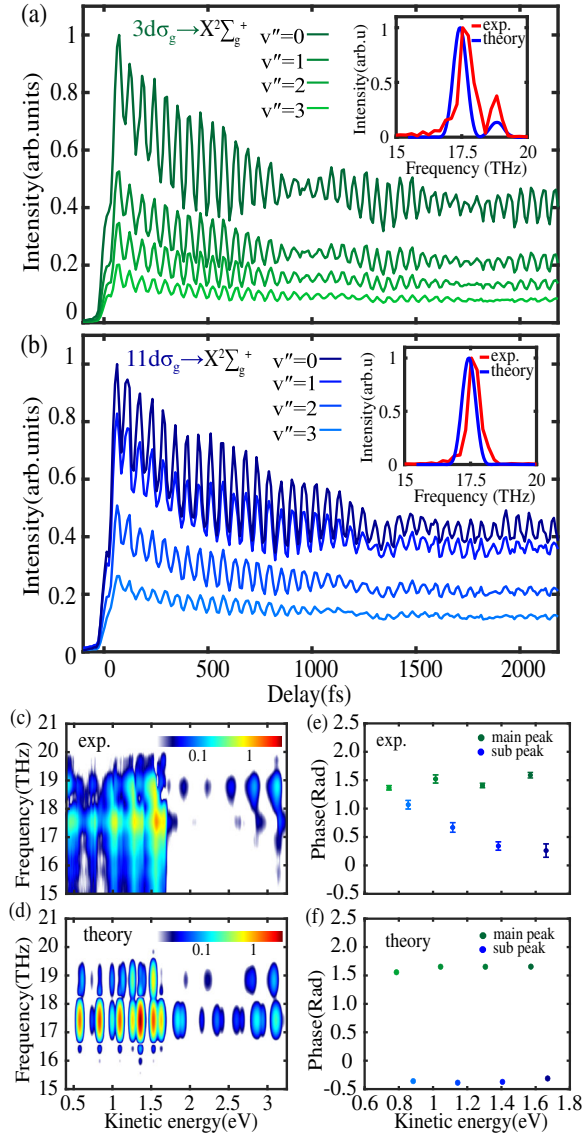


FIG. 2. (a) and (b) The time-dependent photoelectron signals of the transitions from $3d\sigma_g$ ($v'=0$) and $11d\sigma_g$ ($v'=3$) to $X^2\Sigma_g^+$, respectively. The insets in (a) and (b) show the Fourier transform of the oscillating signal [$3d\sigma_g(v'=0) \rightarrow X^2\Sigma_g^+(v''=0)$] and [$11d\sigma_g(v'=3) \rightarrow X^2\Sigma_g^+(v''=0)$] of both experiment (red) and theory (blue), respectively. (c) and (d) Fourier analysis of the observed and calculated TRPES [Figs. 1(b) and 1(d)] as a function of the photoelectron energy with a logarithmic-scale color map, respectively. (e) and (f) Fourier phases of the experimental and simulated two-NIR-photon signal at 17.5 THz, respectively.

simultaneously prepared by the XUV pulse. Referring to the inset in Fig. 2(b), for the subpeaks, only one dominant frequency around 17.5 THz is observed, which is explained below.

As discussed above, the subpeaks appear earlier than the main peaks in the two-NIR-photons region outside the cross-correlation time. This can be further quantified using the common frequency at 17.5 THz from the Fourier

analysis in Fig. 2. The argument extracted from the complex amplitude of the fast Fourier transform spectral components is defined as the phase, which defines the time at which a specific signal maximizes. The extracted phases are presented in Fig. 2(e). The main-peak phases (green dots) are more or less constant at about 1.5 rad, whereas the subpeak phases (blue dots) have a decreasing trend (in absolute value) with increasing its kinetic energy. Overall, this leads to an increasing phase difference between the main and subpeaks with kinetic energy. As such, the population of higher vibrational levels leads to a decrease of the relative time delay between the main and subpeaks. Similarly, Fig. 2(f) shows phases retrieved for the calculated spectrum. Interestingly, the calculations confirm the flat phases for the main peaks and they also reproduce the large phase difference between the main and subpeaks at high kinetic energies. Therefore, the calculations correctly capture the different effects of the autoionizing resonances on the observation of the vibrational wave packet. Interestingly, the calculated subpeak phases stay flat as a function of kinetic energies, whereas the experimental data show a decreasing trend [see Fig. 2(e)]. For the main peaks, on the one hand, the relative contributions of the direct ionization pathways are smaller than those from the autoionization pathways, which is inferred from their relative energy distributions in Fig. 1(a); on the other hand, the phase differences between the direct and the autoionization pathways are overall small (see Fig. S2 in Supplemental Material [43]), such that the observed phases do not vary much as a function of kinetic energy. For the subpeaks, the direct and indirect pathway phase differences are large, and the direct ionization channel becomes dominant at low kinetic energies owing to the increase of photoionization cross sections toward the threshold, which results in a significant modulation on the observed phase with decreasing photoelectron energy (see the analytical estimation in the Supplemental Material [43]). Therefore, the main reason for the discrepancy between the experimental and simulated phases is attributed to the absence of direct photoionization pathways in the simulation.

The above-mentioned observations can be summarized into an intuitive mechanism behind the observation of wave-packet dynamics probed through the autoionizing resonances. The mechanism is depicted in Fig. 3 where the relevant PECs are shown. In the pump step, the XUV pulse centered around 14.15 eV creates a superposition of three vibronic states $b' \ ^1\Sigma_u^+(v'=14, 15, \text{ and } 16)$ (solid red lines) through vertical excitation from the ground state $X^1\Sigma_g^+(v'=0)$.

During the cross-correlation time, the NIR-probe pulse launches the wave packet from b' state to both $3d\sigma_g$ ($v'=0$) and $11d\sigma_g$ ($v'=3$) Rydberg states, since the wave packet is still relatively well localized on the b' state in the FC region. In this situation, the vibrational wave packet formed from the three high-lying vibrational levels

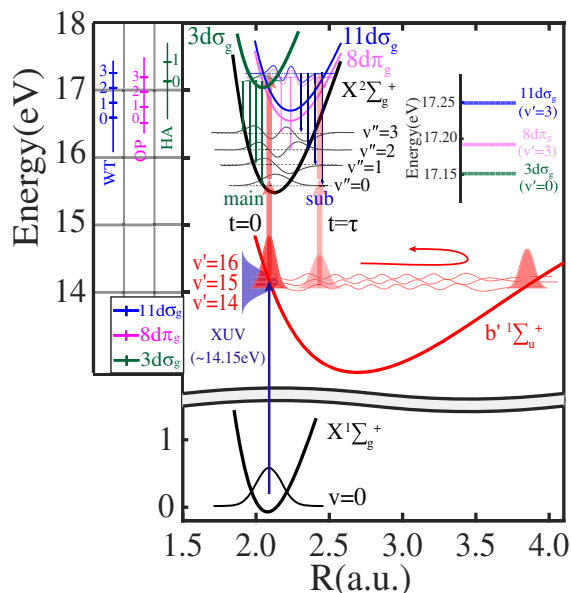


FIG. 3. Schematic PECs in the energy region of interest [33,38]. The ground state of N_2 $X^1\Sigma_g^+$, ionic ground state N_2^+ $X^2\Sigma_g^+$, valence b' $^1\Sigma_u^+$ state, Rydberg state $11d\sigma_g$ and previously assigned Ogawa progression $8d\pi_g$ both converging to $A^2\Pi_u N_2^+$, and Rydberg state $3d\sigma_g$ converging to $B^2\Sigma_u^+ N_2^+$. HA: Hopfield absorption series [36,37,40]. OP: Ogawa progression [36,37,41]. WT: Worley third series [36,47].

($v' = 14, 15, 16$) in the b' state and the $v' = 0$ in $3d\sigma_g$ state have large FC factors irrespective of the internuclear distance R . In contrast, the $v' = 3$ vibrational level of the $11d\sigma_g$ Rydberg state has several nodes, meaning that the corresponding FC factors strongly depend on the internuclear distance R . In addition, the resonant transition between b' ($v' = 14$) and $11d\sigma_g$ ($v' = 3$) could be suppressed as a consequence of the fact that their energy difference (~ 3.17 eV) is slightly larger than the total energy of two NIR photons (~ 3.11 eV). Considering these two aspects, the subpeaks show a negligible contribution from the lowest b' ($v' = 14$) state. Since the two Rydberg states have much shorter lifetimes [20,48] than the cross-correlation, the launched wave packet instantaneously autoionizes to the N_2^+ $X^2\Sigma_g^+$ state. As a result, the main and subpeaks appear at the same time in the spectrum.

At time delays longer than the cross-correlation, an XUV-prepared wave packet passes through the outer turning point of the b' state, see Fig. 3. During its passage back to the inner turning point, a transition between the b' state and the outer turning point of the $11d\sigma_g$ state occurs before a transition to the $3d\sigma_g$ state. This means that the subpeaks generally reach their maxima earlier than the main peaks in the time-resolved spectra beyond the cross-correlation time. Nevertheless, since the direct ionization pathway becomes dominant as the vibrational levels in the $X^2\Sigma_g^+$ ground state of N_2^+ increase toward the ionization threshold, the

interference between the two pathways leads to a significant variation of the observed phases. In contrast, the indirect pathway is always dominant for the main peaks, which results in the observed phases being largely constant for all accessed final states. The internuclear-distance-dependent FCs between the autoionizing states and the ionic states mainly affect the relative intensity of individual peaks, which could also essentially contribute to the interference term and the final-state dependence of the observed phases.

In summary, we have used TRPES to access the ultrafast wave-packet dynamics of N_2 , probed through autoionizing Rydberg resonances with high temporal and spectral resolution. The observed photoelectron spectrum shows clear beating signals, and is well interpreted by a time-dependent quantum-mechanical calculation. Three dominant high-lying adjacent vibrational levels ($v' = 14, 15, 16$) in the b' valence state were prepared by the XUV pulse centered at 14.15 eV. Three autoionizing Rydberg states converging to the $A^2\Pi_u$ and $B^2\Sigma_u^+$ states of N_2^+ were then accessed by the NIR pulse and their signatures are identified in the spectrum, revealing interesting differences in both the phase and the amplitude of the observed b' -state wave-packet signals. This combined experimental and theoretical study demonstrates the important role of autoionizing resonances in TRPES of molecular wave packets and clarifies how these resonances affect the observables of TRPES. The insight gained from this work will support the design and interpretation of future experiments in this field.

This work was supported by ETH Zurich, the Swiss National Science Foundation through the NCCR-MUST, and Project No. 200021_172946. Work by A. T. L. was supported by the U.S. Department of Energy, Office of Science, Office of Basic Energy Sciences under Award No. DE-SC0023192.

*These authors contributed equally to this work.

†pengju.zhang@phys.chem.ethz.ch

‡Present address: Institute of Atomic and Molecular Physics, Jilin University, 130012 Changchun, People's Republic of China.

§Present address: JILA, University of Colorado, Boulder and the National Institute of Standards and Technology, Boulder, Colorado 80309, USA.

||thu.le@uconn.edu

- [1] A. H. Zewail, *J. Phys. Chem. A* **104**, 5660 (2000).
- [2] F. Krausz and M. Ivanov, *Rev. Mod. Phys.* **81**, 163 (2009).
- [3] F. Légaré, K. F. Lee, I. V. Litvinyuk, P. W. Dooley, A. D. Bandrauk, D. M. Villeneuve, and P. B. Corkum, *Phys. Rev. A* **72**, 052717 (2005).
- [4] A. S. Alnaser, B. Ulrich, X. M. Tong, I. V. Litvinyuk, C. M. Maharjan, P. Ranitovic, T. Osipov, R. Ali, S. Ghimire, Z. Chang *et al.*, *Phys. Rev. A* **72**, 030702(R) (2005).

- [5] B. Feuerstein, T. Ergler, A. Rudenko, K. Zrost, C. D. Schröter, R. Moshhammer, J. Ullrich, T. Niederhausen, and U. Thumm, *Phys. Rev. Lett.* **99**, 153002 (2007).
- [6] F. Kelkensberg, C. Lefebvre, W. Siu, O. Ghafur, T. T. Nguyen-Dang, O. Atabek, A. Keller, V. Serov, P. Johnsson, M. Swoboda *et al.*, *Phys. Rev. Lett.* **103**, 123005 (2009).
- [7] P. M. Kraus, A. Rupenyan, and H. J. Wörner, *Phys. Rev. Lett.* **109**, 233903 (2012).
- [8] P. M. Kraus, D. Baykusheva, and H. J. Wörner, *Phys. Rev. Lett.* **113**, 023001 (2014).
- [9] P. M. Kraus, B. Mignolet, D. Baykusheva, A. Rupenyan, L. Horný, E. F. Penka, G. Grassi, O. I. Tolstikhin, J. Schneider, F. Jensen *et al.*, *Science* **350**, 790 (2015).
- [10] Y. Nabekawa, Y. Furukawa, T. Okino, A. A. Eilanlou, E. J. Takahashi, K. Yamanouchi, and K. Midorikawa, *Nat. Commun.* **7**, 12835 (2016).
- [11] D. R. Cyr and C. C. Hayden, *J. Chem. Phys.* **104**, 771 (1996).
- [12] D. M. Neumark, *Annu. Rev. Phys. Chem.* **52**, 255 (2001).
- [13] T. Suzuki, L. Wang, and M. Tsubouchi, *J. Phys. Chem. A* **108**, 5764 (2004).
- [14] G. Wu, P. Hockett, and A. Stolow, *Phys. Chem. Chem. Phys.* **13**, 18447 (2011).
- [15] A. von Conta, A. Tehlar, A. Schletter, Y. Arasaki, K. Takatsuka, and H. J. Wörner, *Nat. Commun.* **9**, 3162 (2018).
- [16] M. Koch, T. J. A. Wolf, and M. Gühr, *Phys. Rev. A* **91**, 031403(R) (2015).
- [17] I. Wilkinson, A. E. Boguslavskiy, J. Mikosch, J. B. Bertrand, H. J. Wörner, D. M. Villeneuve, M. Spanner, S. Patchkovskii, and A. Stolow, *J. Chem. Phys.* **140**, 204301 (2014).
- [18] V. Svoboda, N. B. Ram, R. Rajeev, and H. J. Wörner, *J. Chem. Phys.* **146**, 084301 (2017).
- [19] E. R. Warrick, W. Cao, D. M. Neumark, and S. R. Leone, *J. Phys. Chem. A* **120**, 3165 (2016).
- [20] M. Eckstein, C.-H. Yang, F. Frassetto, L. Poletto, G. Sansone, M. J. J. Vrakking, and O. Kornilov, *Phys. Rev. Lett.* **116**, 163003 (2016).
- [21] L. J. Zipp, A. Natan, and P. H. Bucksbaum, *Phys. Rev. A* **95**, 061403(R) (2017).
- [22] E. R. Warrick, J. E. Bkhj, W. Cao, A. P. Fidler, F. Jensen, L. B. Madsen, S. R. Leone, and D. M. Neumark, *Chem. Phys. Lett.* **683**, 408 (2017).
- [23] C. Marceau, V. Makhija, P. Peng, M. Hervé, P. B. Corkum, A. Y. Naumov, A. Stolow, and D. M. Villeneuve, *Phys. Rev. A* **99**, 023426 (2019).
- [24] M. Fushitani, Y. Toida, F. Légaré, and A. Hishikawa, *Opt. Express* **27**, 19702 (2019).
- [25] M. Fushitani, S. T. Pratt, D. You, S. Saito, Y. Luo, K. Ueda, H. Fujise, A. Hishikawa, H. Ibrahim, F. Légaré *et al.*, *J. Chem. Phys.* **154**, 144305 (2021).
- [26] A. von Conta, M. Huppert, and H. J. Wörner, *Rev. Sci. Instrum.* **87**, 073102 (2016).
- [27] V. Véniard, R. Taieb, and A. Maquet, *Phys. Rev. Lett.* **74**, 4161 (1995).
- [28] S. Xue, H. Du, B. Hu, C. D. Lin, and A.-T. Le, *Phys. Rev. A* **97**, 043409 (2018).
- [29] M. Seel and W. Domcke, *J. Chem. Phys.* **95**, 7806 (1991).
- [30] R. de Vivie-Riedle, K. Kobe, J. Manz, W. Meyer, B. Reischl, S. Rutz, E. Schreiber, and L. Wöste, *J. Chem. Phys.* **100**, 7789 (1996).
- [31] Y. Arasaki, K. Takatsuka, K. Wang, and V. McKoy, *J. Chem. Phys.* **112**, 8871 (2000).
- [32] D. Stahel, M. Leoni, and K. Dressler, *J. Chem. Phys.* **79**, 2541 (1983).
- [33] D. Spelsberg and W. Meyer, *J. Chem. Phys.* **115**, 6438 (2001).
- [34] J. S. Ajay, K. G. Komarova, F. Remacle, and R. D. Levine, *Proc. Natl. Acad. Sci. U.S.A.* **115**, 5890 (2018).
- [35] P. Cremaschi, A. Chattopadhyay, P. Madhavan, and J. Whitten, *Chem. Phys.* **109**, 117 (1986).
- [36] W. M. Kosman and S. Wallace, *J. Chem. Phys.* **82**, 1385 (1985).
- [37] L.-E. Berg, P. Erman, E. Kllne, S. Sorensen, and G. Sundström, *Phys. Scr.* **44**, 131 (1991).
- [38] D. A. Little and J. Tennyson, *J. Phys. B* **46**, 145102 (2013).
- [39] W. C. Ermler, J. P. Clark, and R. S. Mulliken, *J. Chem. Phys.* **86**, 370 (1987).
- [40] M. Raoult, H. L. Rouzo, G. Raseev, and H. Lefebvre-Brion, *J. Phys. B* **16**, 4601 (1983).
- [41] M. Ogawa, *Can. J. Phys.* **42**, 1087 (1964).
- [42] P. Peng, C. Marceau, M. Hervé, P. B. Corkum, A. Y. Naumov, and D. M. Villeneuve, *Nat. Commun.* **10**, 5269 (2019).
- [43] See Supplemental Material at <http://link.aps.org/supplemental/10.1103/PhysRevLett.130.153201> for a detailed account of the relative time differences between main- and subpeaks, the phases of the direct pathways, and an analytical model for the interference between direct and indirect pathways.
- [44] R. Robinett, *Phys. Rep.* **392**, 1 (2004).
- [45] P. Cörlin, A. Fischer, M. Schönwald, A. Sperl, T. Mizuno, U. Thumm, T. Pfeifer, and R. Moshhammer, *Phys. Rev. A* **91**, 043415 (2015).
- [46] H. Lefebvre-Brion and C. M. Moser, *J. Chem. Phys.* **43**, 1394 (1965).
- [47] J. B. Randazzo, P. Croteau, O. Kostko, M. Ahmed, and K. A. Boering, *J. Chem. Phys.* **140**, 194303 (2014).
- [48] M. Reduzzi, W.-C. Chu, C. Feng, A. Dubrouil, J. Hummert, F. Calegari, F. Frassetto, L. Poletto, O. Kornilov, M. Nisoli *et al.*, *J. Phys. B* **49**, 065102 (2016).